Colloid Polym Sci 278:954–963 (2000)

ORIGINAL CONTRIBUTION

R. Sabia
K. Powers
J. H. Adair

Formation and analysis of particulate carbon in a synthetic lubricant

Received: 29 February 2000
Accepted: 3 January 2000

R. Sabia (✉)[1] · K. Powers · J. H. Adair[2]
Materials Science and Engineering
University of Florida
Gainesville, FL 32601, USA

Present addresses:
[1] Corning Incorporated
Corning, NY 14831, USA
e-mail: sabiar@corning.com
Tel.: +1-607-974-5073
Fax: +1-607-974-2925

[2] Pennsylvania State University
University Park, PA 16802, USA

Abstract The formation of discrete carbonaceous particles has been investigated for a conventional synthetic ester-based lubricant degraded in thermal and thermal–oxidative environments. Experimental factors included oxidative and nonoxidative environments, high and low humidities, and the presence or lack of a metal catalyst surface, with all samples generated at 250 °C. Characterization performed for changes in antioxidant content, IR spectroscopy, molecular weight, total acid number, viscosity, and uv/vis absorbance spectrometry were used to determine the influences of the aforementioned variables on the rates of oil degradation and formation of high-molecular-weight species. Discrete carbonaceous particle formation was analyzed using Einstein's relationship for the viscoelastic behavior of particles in Newtonian fluids and by calculating associated radii of gyration. This viscoelastic behavior of the particles in solution is used to demonstrate how the absorption behavior of the carbonaceous degradation products tracks the discrete particulate species. The results show the formation of particulate species to be diffusion-limited after antioxidant depletion, and optical absorption analysis is shown to be a viable technique for monitoring the formation of discrete carbonaceous particles during lubricant degradation.

Key words Carbonaceous particles · Degradation · Esters · Optical absorption · Soot

Introduction

For bearing applications in aircraft gas-turbine engines, where bulk lubricant operating temperatures range between 75 and 150 °C, boundary and elastohydrodynamic contact temperatures can reach 250–350 °C due to frictional heating [1]. Chemical reactions, which are normally nonexistent or which occur at a low rate, can be accelerated under these temperature conditions [2]. When operating for an extended time at temperatures over 200 °C, most commercial ester-based lubricants oxidize, polymerize, or evaporate [3]. The most common mechanisms for the degradation of these ester-based lubricants are thermal and thermal–oxidative degradation, as well as tribochemical degradation [4]. A further intensifying degradative condition is the behavior of a gas-turbine engine in acting as an "open" system by incorporating air for oil pressure control [5].

Both thermal and thermal–oxidative degradation processes consist of free-radical chain mechanisms [6–7] in which free radicals act to polymerize lubricant constituents by initiating reaction chains via abstraction of hydrogen atoms from parent molecules [8]. Free-radical chain propagation is the most detrimental oil degradation mechanism and is in part controlled by the addition of antioxidant additives. Antioxidants act to eliminate chain propagation by donating a proton to the free radicals, therefore rendering them inactive. The antioxidant molecule then becomes a free radical which is self-stabilized through resonance [6–7]. Once the

antioxidant is depleted, degradation accelerates unchecked and results in the formation of soot, a mixture of discrete carbonaceous particles and various organic and inorganic components [9]. After formation, the carbonaceous particles (i.e., soot) coat bearing components, significantly altering performance [10].

The purpose of the research at hand was to investigate the formation of degradation products in a synthetic ester-based lubricant, including determining the kinetics of reactions both before and after antioxidant depletion. Special emphasis was given to determining to what extent the degradation products acted as discrete particles and to the ability of using optical absorption as a technique for monitoring the formation of the degradation products.

Experimental

A series of experiments was performed under varying environmental conditions promoting thermal and thermal–oxidative degradation. As shown in Table 1, eight experimental conditions were tested in varying atmosphere, humidity, and the presence of M-50 steel surfaces. For each test, 750 ml of as-received synthetic ester-based oil (MIL-L-23699C) was heated in a glass beaker on a hot plate with a constant-temperature controller. The thermocouple of the controller was covered with a sealed glass capillary tube to avoid catalytic degradation created by the probe's metal surface. Gas flow and oil turbidity were provided using a glass dispersion tube with a flow rate of 0.83 l/min. In this manner, the oil was completely isolated from metallic surfaces which might act as catalysts. The heating rate was approximately 225 °C/h to 250 °C.

In accordance with Table 1, the gas supplied in each experiment was either compressed argon, resulting in an inert (nonoxidative) atmosphere allowing thermal degradation without oxidation, or compressed air, allowing both thermal and oxidative degradation. M-50 steel was supplied as a catalyst material for designated tests in the form of 0.25-in. diameter ball bearings placed in the oil bath. The resulting ratio of available surface area to oil was 3.6 mm^2/ml. For tests performed under low humidities, the relative humidity for both compressed argon and air was determined using an on-line sensor to be 12% or less. For tests performed under high humidity, a liquid bubbler filled with distilled water was utilized, resulting in relative humidities for the gas entering the bath of 85% for argon and 92% for air. Samples were generated for test times of 3, 5, 7, 9, and 13 h, with each sample representing an independent experiment (40 in total) and samples for each test time reflecting a 2^3 factorial design [11]. In this report, each test series is coded as shown in Table 1.

Table 1 Conditions for degradation experiments, representing a 2^3 factorial design. Experimental codes are indicated in terms of inert (*IN*) or oxidative (*OX*) environments, low (12) or high (85 or 92) percent humidity, and the presence of (*C*) or lack of (*NC*) a catalyst surface. Samples were generated for each condition at 3-, 5-, 7-, 9-, and 13-h test times, thus producing samples from 40 independent experiments

Test ID	Temperature (°C)	Atmosphere	Humidity %	Catalyst
IN12NC	250	Inert	<12	None
IN12C	250	Inert	<12	M-50
IN85NC	250	Inert	~85	None
IN85C	250	Inert	~85	M-50
OX12NC	250	Oxidative	<12	None
OX12C	250	Oxidative	<12	M-50
OX92NC	250	Oxidative	~92	None
OX92C	250	Oxidative	~92	M-50

Characterization of the degraded oil samples was performed to obtain insight into the physical and chemical changes generated in the oil samples. Viscosity measurements were performed using a variable-speed cone-and-plate viscometer at 40 ± 0.1 °C, with measurements made at shear rates between 0.75 and 450 s^{-1}. The concentration of the antioxidant additive was determined using the Remaining Useful Lubricant Life Evaluation Rig (University of Dayton Research Institute, Dayton, Ohio). The extent of degradation as indicated by the acid content was determined by titration for total acid number (TAN) (ASTM 664-89). Spectrometric analysis was performed using transmission Fourier transform IR spectroscopy with a nitrogen purge and analyzing chemical changes in characteristic vibrational peaks. Molecular-weight (MW) analysis was determined by size-exclusion chromatography using columns covering the 50–300,000 MW range, a UV/vis detector at 216-nm, tetrahydrofuran as the solvent carrier, and polystyrene standards in toluene for calibration. Evaluation of changes in peak-intensities and locations was performed using peak-separation and analysis software assuming Gaussian distributions.

Optical absorption spectroscopy was performed using a UV/vis/near-IR spectrometer, in which oil samples were analyzed in constant path length cells for absorbance with ±0.1% accuracy between 350 and 2000-nm, covering the uv, visible, and near-IR regions of the electromagnetic spectrum. In order to analyze the absorption behavior of the degrading oil and to determine if the Beer–Lambert law [12–13] was followed for the absorption behavior of concentrated samples, the 13-h sample from test OX12NC was diluted in as-received oil and was appropriately analyzed.

Results

Environmental effect on degradation

The bulk lubricant physical and chemical changes resulting from degradation were analyzed in terms of viscosity changes, antioxidant content, and acid content. The viscosity measurements showed all oil samples to yield Newtonian behavior without Bingham yield points. The oil viscosity increased with test time for each test series (Fig. 1a), with more dramatic increases in oxidative environments (above 100% maximum change) compared to nonoxidative environments (25–30% maximum change). The presence of the M-50 steel caused extremer changes in viscosity, whereas higher humidity produced less extreme changes, particularly for those samples tested in oxidative environments. The influence of increased humidity in hindering degradation suggests the degradation mechanism to be condensation. The results for antioxidant content and TAN (Fig. 1b, C, respectively) showed similar changes to those for viscosity. For increasing test time, the extent to which degradation had occurred is indicated by increasing TAN values and the potential for continued degradation is indicated by decreasing antioxidant content. The

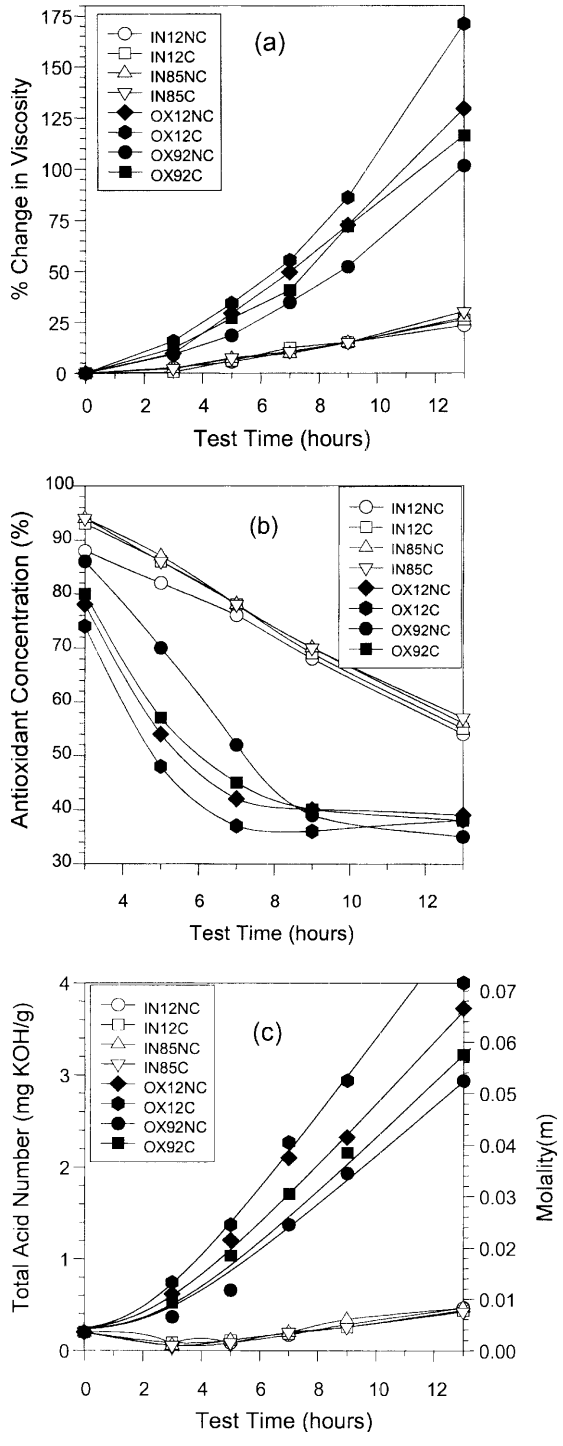

Fig. 1 Changes in **a** viscosity **b** antioxidant content, and **c** total acid number (*TAN*) as a function of test time for lubricant samples degraded in various environments. All 40 data points represent independent experiments, and estimation of the variance for the 2^3 factorial designs indicates significant changes in viscosity and TAN after 9 h and in antioxidant content after 5 h for tests performed in oxidative environments

variations in the rate of change for TAN values and in antioxidant content with respect to the presence of catalyst and humidity were consistent with viscosity changes, where maximum changes for the 13-h test samples yielded TAN and antioxidant values of 0.45 and 55%, respectively, for nonoxidative environments and 4.0 and less than 40%, respectively for oxidative test environments. Statistical verification of these results was performed by estimation of the variance for 2^3 factorial designs [11], indicating that changes in the oxidative environments were significant for viscosity and TAN values at test times of 9 h or more and for antioxidant content at test times of 5 h or more.

Vibrational analysis of degraded samples

The results from IR analysis for the as-received oil yielded strong absorption peaks between 2850 and 3000 cm^{-1} and a weak peak at 1465 cm^{-1}, all reflecting hydrocarbon stretches. A strong peak at 1743 cm^{-1} represented one or more carbonyl peaks for ester structures within the base oil, and a variety of lower intensity peaks between 1000 and 1465 cm^{-1}, which included the C-C(=O)-O (lactone) and the O-C-C peaks [14], were not distinguishable. For the degraded oil samples, peak broadening with test time was observed for the carbonyl peak, suggesting the generation of new carbonyl peaks for which transesterification and the formation of ketones or carboxylic acids are possible.

MW analysis

The size-exclusion chromatography results are presented for the IN12NC test samples in Fig. 2. Six peaks were found for the as-received oil sample, with MW of 215, 267, 432, 662, 863, and 1292. In order to determine how the MW distributions changed with test time, peak separation and analysis ($r^2 \geq 0.996$) was performed using Gaussian curve fitting for each of the tests. The changes in the MW distributions showed decreases in intensities for the four lowest MW peaks and increases in intensities for the two highest peaks. The peaks which underwent the greatest changes were the 1292 MW and 267 MW peaks.

Absorption behavior of degraded oil samples

Absorption analysis of the degraded oil samples generated for this study was performed using a high-performance uv/vis spectrometer capable of detecting absorption characteristics in the near-IR spectral region. Samples were tested to higher wavelengths within the IR region in order to discern between absorption and Mie

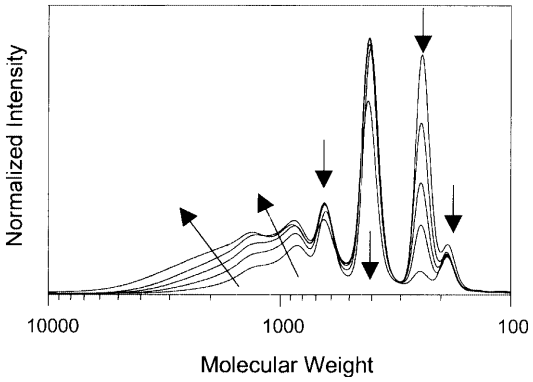

Fig. 2 Molecular-weight (*MW*) chromatogram curves for test series IN12NC (inert environment with 12% relative humidity and no catalytic surface present). *Arrows* indicate changes in peak heights with increasing test times. Of particular note are the 267 MW peak, representing the antioxidant and the 1292 MW peak, representing the carbonaceous degradation product. With increasing test time, the 1292 MW peak increased in peak fitted area and mean MW value

Table 2 List of concentrations (weight percent) and normalized absorbance peak areas (given in percent change) for OX12NC 13-h test sample diluted in as-received oil

Concentration (wt%)	355-nm peak area (%)	415-nm peak area (%)	500-nm peak area (%)
0.36	−28	86	200
0.54	−32	136	220
0.66	−40	157	300
0.85	−44	176	520
2.09	−50	597	900
4.95	–	1610	2650
9.45	–	3189	4100
29.12	–	7400	6900
50.00	–	13,058	14,900
75.00	–	19,637	19,900
100.00	–	23,584	21,900

scattering effects. Once it was confirmed that spectrographic changes were the result of absorption effects rather than scattering, characterization of absorbance peaks was performed by diluting portions of the 13-h sample from the OX12NC test in as-received oil to the concentrations shown in Table 2. The results are shown in Fig. 3a, where the absorbance of the solutions it seen to increase and the loss edge shifts to higher wavelengths with increasing concentration, as indicated by the arrow.

The changes in absorption behavior have been attributed to the presence of three absorption peaks, located at 355, 415, and 500-nm. The peaks were fitted for Gaussian distributions as shown in Fig. 3b, where the 355-nm peak is initially highly absorbing and decreases in intensity as the concentration of the degraded oil increases. The 415- and 500-nm peaks are initially not strongly absorbing, but increase in

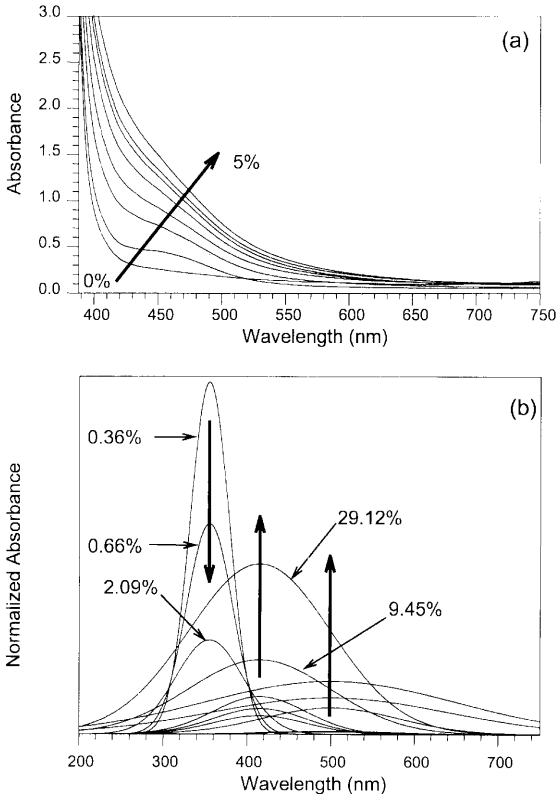

Fig. 3 Changes in the absorbance spectra for the OX12NC, 13-h sample diluted in as-received oil as a function of **a** concentration and **b** changes in intensities for the 355-, 415-, and 500-nm peaks with changes in concentration

absorbance with increasing concentration of the degraded oil. In Fig. 3b, the most absorbing peaks for the indicated concentration are identified. For dilutions of 2.09% and below, the 355-nm peak is dominant, whereas for concentrations of 9.45% and above, the 415-nm peak is most absorbing. These results show that the absorbance spectra reflect the extent of oil degradation, but only after a certain amount of degradation has occurred and a large enough concentration of degradation species exists.

Discussion

Degradation product formation and antioxidant depletion

The significance of changes for the 1292 MW and 267 MW peaks can be understood from observation of a number of correlations. The changes in viscosity and TAN are plotted in Fig. 4a and b versus the formation of high-MW species reflected by the increasing area of the 1292 MW peak. Fitted curves are presented in each graph, representing both nonoxidative and oxidative

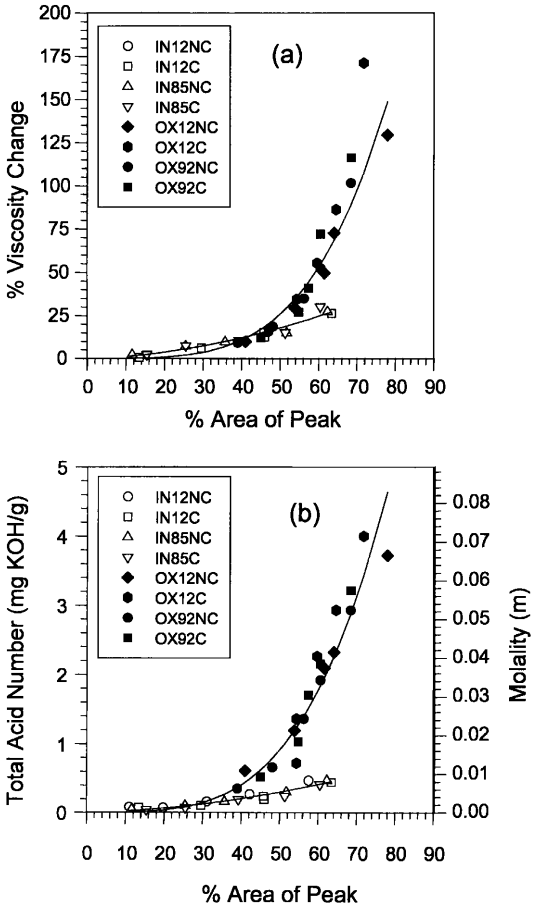

Fig. 4 **a** Viscosity and **b** TAN versus changes in percentage area of the 1292 MW peak. *Plotted lines* correspond to oxidative environments and nonoxidative environments

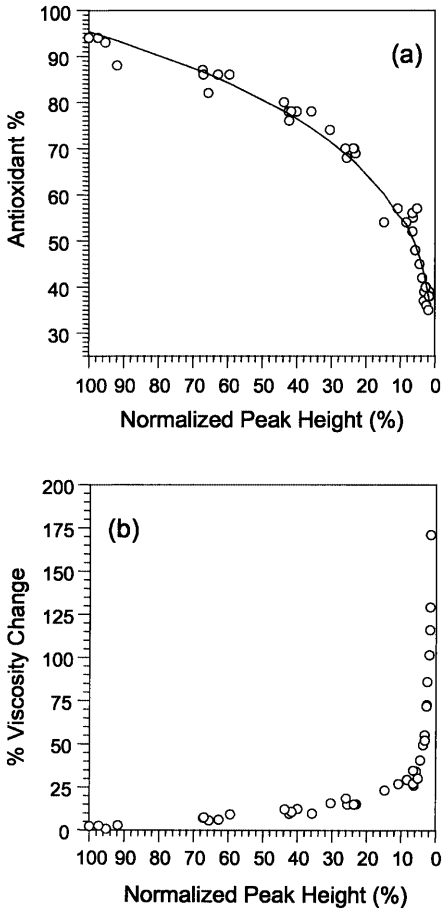

Fig. 5 **a** Changes in antioxidant content versus normalized height for the 267 MW *peak* and **b** changes in viscosity versus normalized height for the 267 MW peak. The results show the viscosity increases significantly after removal of the 267 MW antioxidant peak, corresponding to a 40–45% antioxidant context

environments. The two curves deviate at about 55% peak area in both graphs, showing dramatic increases in peak area beginning for oxidative testing at 25% viscosity change and about 0.5 mg KOH/g. These results show increases in MW began at the same peak area for both viscosity and TAN values, suggesting that viscosity and MW changes are a direct result of oil degradation. The importance of this correlation will be shown when relating viscosity to concentration of particulate species later.

Similar correlations were made with changes in intensities for the 267 MW peak. Decreasing peak height directly correlates with decreasing antioxidant content (Fig. 5a), thus showing that the species represented by the 267 MW peak is in fact the antioxidant. A second correlation for the 267 MW peak is shown in Fig. 5b, where peak height is plotted versus changes in viscosity. The viscosity increased at a constant rate to 25% change, reflected by a 267 MW peak height of 10% before increasing more significantly. Thus, increasing viscosity was not dependent on the removal of a low-MW species (as is one possibility), but was rather completely dependent on the depletion of the antioxidant. Furthermore, Fig. 5b shows that the effectiveness of the antioxidant is lost when the 267 MW peak height has dropped to approximately 10%, thus correlating with Fig. 5a to an antioxidant concentration between 55 and 60%.

Rate of degradation product formation

The effects that humidity and presence of catalyst have on the actual rate (kinetics) of degradation can be determined. A measure of the degree of degradation generated for the 1292 MW peak was calculated as follows:

$$\text{Growth factor} = \text{mean MW} \times \text{normalized peak area}, \quad (1)$$

where normalized peak area is the fraction of the total area occupied by the 1292 MW peak calculated from the fitted Gaussian distributions and the growth factor represents the size and arbitrary concentration of high-MW degradation products. The rate of degradation was then determined by plotting the growth factor versus test time for each test series (Fig. 6a), with the linear correlation coefficients ($r^2 \geq 0.985$) and slopes for each test series listed in Table 3. However, the peak area does not represent absolute concentration since MW analysis is performed at only one wavelength. Thus, the exact concentration of high-MW degradation products is unknown and the rate constants cannot be calculated for each test series.

Discrete particle formation

Since the viscosity measurements for all samples reflected Newtonian behavior, the Einstein relationship for the viscoelastic behavior of particles in Newtonian fluids [15] was used to determine the physical behavior of the high-MW degradation products

$$\eta^* = \eta_0(1 + \tfrac{5}{2}\phi) \tag{2}$$

η^* refers to the experimental viscosity, η_0 refers to the as-received viscosity, and ϕ refers to the percent particle volume of the system. In Fig. 6b, the particle content calculated from Eq. (2) is shown to correlate with changes in the high-MW degradation product represented by the growth factor (Eq. 1). These results confirm that the degradation product acts as a discrete particulate species with respect to physical changes shown by changes in viscosity.

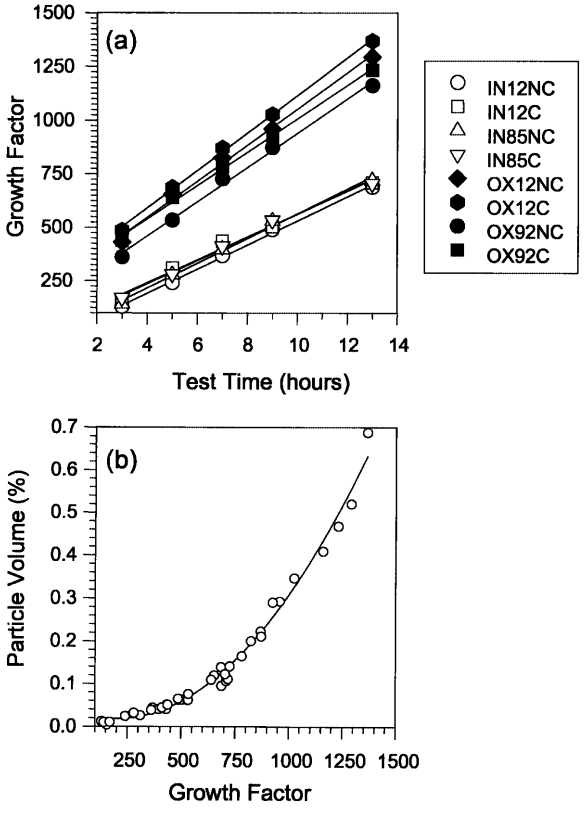

Fig. 6 **a** Rate of growth for high-MW degradation species, showing a linear relationship between the carbonaceous degradation product (Initial peak location at 1292 MW) and test time, thus representing a higher-order kinetics reaction. **b** The plot of particle volume (Eq. 2) and growth factor (Eq. 1) shows a continuous change in particle concentration, thus demonstrating that the degradation product behaves as discrete particles in suspension. The correlation coefficient is $r^2 = 0.987$

Table 3 List of correlation coefficients and slopes for the plot of growth factor versus test time shown in Fig. 6a

Test ID	Correlation coefficient (r^2)	Slope (m)
IN12NC	0.997	56.4
IN12C	0.985	53.6
IN85NC	0.993	57.8
IN85C	0.992	54.3
OX12NC	0.994	84.1
OX12C	0.998	87.3
OX92NC	0.996	79.9
OX92C	0.996	77.7

In order to understand the kinetics information generated and presented using the growth factor (Eq. 1), the rate-determining and rate-limiting mechanisms of Overbeek [16] were reviewed. Overbeek gave definitions for rates of reactions when diffusion is rate-determining. Information was presented in terms of mean particle size and particle size distribution. In order to apply this information to the present work, calculations were made to estimate the particle size of the high-MW degradation products using radii of gyration [17]:

$$r_g = \frac{l\sqrt{\frac{MW}{M_0}}}{\sqrt{6}} \quad . \tag{3}$$

r_g is the radius of gyration, l refers to the bond length, MW is the chain MW, and M_0 is the monomer MW. Since the repeating units for the base ester structures are ethylene and the standards used to calibrate the gel permeation chromatography columns were polystyrene, the monomer weight of polyethylene ($M_0 = 28$) and the bond length for polystyrene ($l = 0.53$ nm) were used for the calculations to estimate the radii of gyration for the high-MW degradation products.

The changes in the mean MW values for the high-MW degradation product (1292 MW peak) versus changes in the MW distributions for the fitted Gaussian peaks taken from the full width at half maximum are plotted in Fig. 7. Estimated values for the radii of

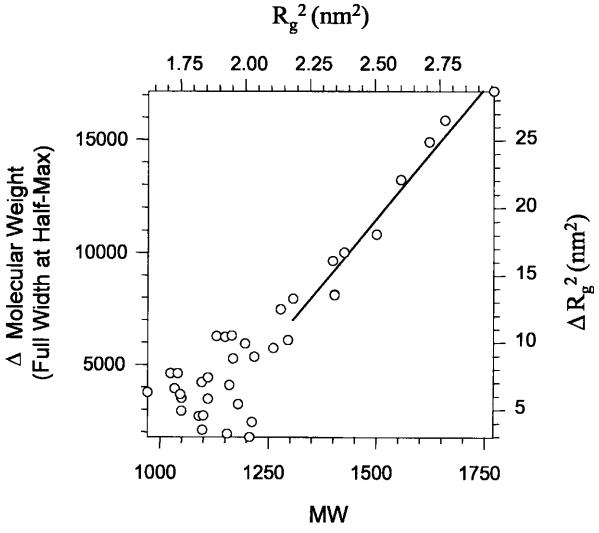

Fig. 7 Changes in MW distribution versus MW, including the corresponding values for the radius of gyration (Δr_g^2 and r_g^2, respectively) for the carbonaceous degradation product. The results indicate that the reaction to form the carbonaceous particles is diffusion-limited after antioxidant depletion

gyration calculated using Eq. (3) are also included (MW $\sim$ r_g^2). During the initial stage of oil degradation (i.e., prior to antioxidant removal indicated in Fig. 7 at MW$\sim$1300), changes in particulate size do not correlate with particulate size distribution and thus no information can be determined as for the rate-limiting effects. After the antioxidant is removed the changes become linear, indicating the availability of rate-determining information after antioxidant is depleted. From Fig. 6a, the mean MW and, thus, the particle radius squared change linearly with time, following the relationship

$$a^2 = kt + b \ , \tag{4}$$

where a refers to the particle size and k and b are constants. Differentiation of Eq. (4) shows that changes in the mean MW (particle size) follow the kinetics relation

$$\frac{da}{dt} = k' a^{-1} \ , \tag{5}$$

where k' is a constant. In accordance with the work presented by Overbeek, Eq. (5), the relation for diffusion-limiting growth is

$$\frac{da}{dt} = \frac{D(c_\infty - c_0)V}{a^n} \ , \tag{6}$$

where D is the diffusion coefficient, V is the molar volume, $(c_\infty - c_0)$ is the change in concentration, and n can be 2, 1, 0, and -1. These results show that once the antioxidant is removed, degradation in the oil system resulting in the formation of particulate carbon residue is diffusion-limited.

Absorption behavior and particulate concentration

The changes in the absorption behavior of the degraded oil sample diluted in as-received oil (shown in Fig. 3) suggest that the absorption characteristics are directly related to the concentration of the degradation products. In order to test this hypothesis, the Beer–Lambert law was evaluated for this oil system. The changes in peak area as a function of concentration were calculated from fitted Gaussian distributions and were used for absorbance values (listed in Table 2). The changes in absorbance peak area as a function of concentration for the 415- and 500-nm absorption peaks are shown in Fig. 8 Both peaks yield linear results and thus conform to the Beer–Lambert law.

The results shown in Fig. 8 yielded slopes for both peaks which are approximately equal ($m = 4.1$ and 4.2 for the 415- and 500-nm peaks, respectively), suggesting that both peaks are due to the same degradation product. However, Fig. 9a shows the absorption characteristic for the 415- and 500-nm peaks plotted versus changes in the high-MW degradation product. Both absorption peaks follow the same general trend until approximately 45% peak area, at which the absorbance values for the 500-nm peak undergo positive deviation with respect to the 415-nm peak. Further comparison is made in Fig. 9b, where the absorbance peak data is plotted versus growth factor values. The absorbance values for the 415- and 500-nm peaks increase at equivalent rates until the mean MW values for the degradation products begin to increase, after which the 500-nm absorbance peak undergoes positive deviation with respect to the 415-nm peak. This behavior shows

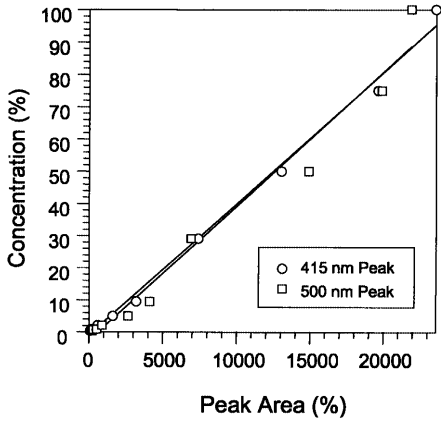

Fig. 8 Absorbance values for the 415- and 500-nm peaks for the OX12NC, 13-h test sample diluted in as-received oil to the concentrations listed in Table 2. The linear regression coefficients and Slopes for the 415 nm and 500 nm peaks are $r^2 = 0.99$, $m = 4.07$ and $r^2 = 0.98$, $m = 4.16$, respectively, showing that the absorption behavior of these peaks follows the Beer–Lambert law for concentrations of high-MW degradation products

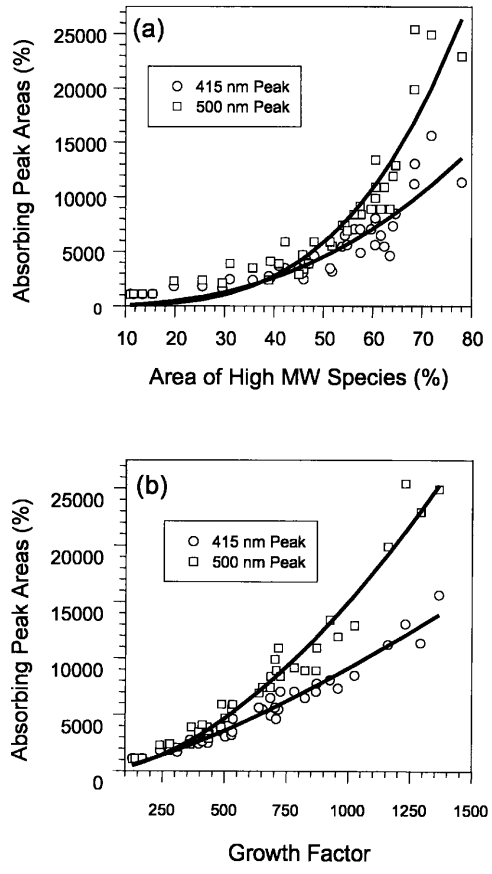

Fig. 9 Changes in absorbance for the 415-nm and 500-nm peak areas with **a** high-MW species (correlation coefficients of $r^2 = 0.93$ and 0.95, respectively) and **b** growth factor values calculated from Eq. (1). The absorbance behavior of the 415 nm peak correlates with the MW peak area, whereas the 500 nm peak represents a combination of MW peak area and mean values

that the 415 nm peak represents the increasing MW peak area for the degradation product, whereas the 500-nm absorbance peak represents both increases in MW area and mean values. Thus the absorbance behavior of the 500-nm peak is more representative of the true oil condition.

Degradation product concentration versus particle volume

From the absorbance information generated for the oil samples, the relative concentration of the absorbing species can be determined by normalizing the absorbance area for a given peak with respect to the most degraded test sample. Although this normalization method does not allow the determination of extinction coefficients associated with absorbing species, it does allow a general description of the extent to which the quantity of degradation product affects the overall absorbance properties of the test samples to be made. Further comparisons can be made with the physical changes associated with oil degradation by treating the high-MW degradation product as particulates. Figure 10 shows the relationship between particle volume as calculated using Eq. (2) and the relative concentration of the degradation species determined for the 415-nm (Fig. 10a) and 500-nm (Fig. 10b) absorbance peaks B. The particle volume calculations yielded maximum values of 0.69%. The concentrations associated with the absorption peaks show linear relationships, with slope and correlation coefficients of $m = 1.34$ and $r^2 = 0.93$ for the 415-nm peak and $m = 1.55$ and $r^2 = 0.92$ for the 500-nm peak. The differences in the slopes support the hypothesis that the two absorbance peaks do not reflect the same behavior. Furthermore, the linear relationships shown in Fig. 10 support the hypothesis that the high-MW degradation products behave as particulate species to increase viscosity in the degraded oil.

Association of absorbance peaks

Identification of the absorbing species reflected by the 355-, 415-, and 500-nm peaks has not been accomplished due to the high number of possible degradation products for synthetic oil systems and the lack of absorption information on each product. However, knowing that the 355- and 415-nm absorption peaks are in the uv region, that only compounds with chromophoric groups, for example, poly(enes) and species with carbonyl and aromatic rings, absorb in this region, and that ester compounds are the primary constituent (above 90%) in the as-received oil allows a general association of the probable absorbing species to be made. Since the

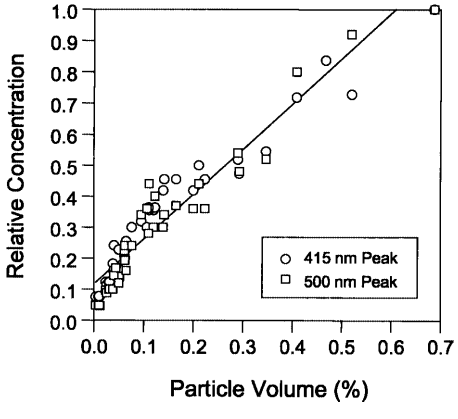

Fig. 10 Relative concentration of high-MW species versus particle volume for the 415-nm absorbance peak, where $r^2 = 0.93$ and $m = 1.34$, and for the 500-nm peak, where $r^2 = 0.92$ and $m = 1.55$. The linear relationships show that the high-MW degradation products act as particulate species

355-nm peak decreases and the 415-nm peak increases, the 355-nm peak can be attributed to the original base esters, which decrease in concentration during the reaction to form degradation products, and the 415- and 500-nm peaks can be attributed to the high-MW degradation products (i.e., particulate species) that contain carbonyl groups.

Reaction kinetics for absorbance peaks

Since the absorbance behavior of the 415- and 500-nm peaks has been shown in Fig. 8 to conform to the Beer–Lambert law, the area under each absorbance curve can be related to the concentration of degradation product. The rate of product generation with test time is shown in Fig. 11a to be linear. To confirm the same behavior for the absorptivity of the 415- and 500-nm peaks, Fig. 11 shows a linear relationship between absorbance and test time. The values for correlation coefficients and slopes are shown in Table 4. Comparison of this data with the results for the previously reported growth factor analysis shows lower correlation coefficients for the absorption peaks, an indication of less accurate measurements which is attributed to human error involved in selection of absorbance peak values. Further comparison of the slope values shown in Table 4 yields linear correlation coefficients of 0.92 or greater, confirming that the absorbance peak information accurately reflects the concentration of high-MW degradation products.

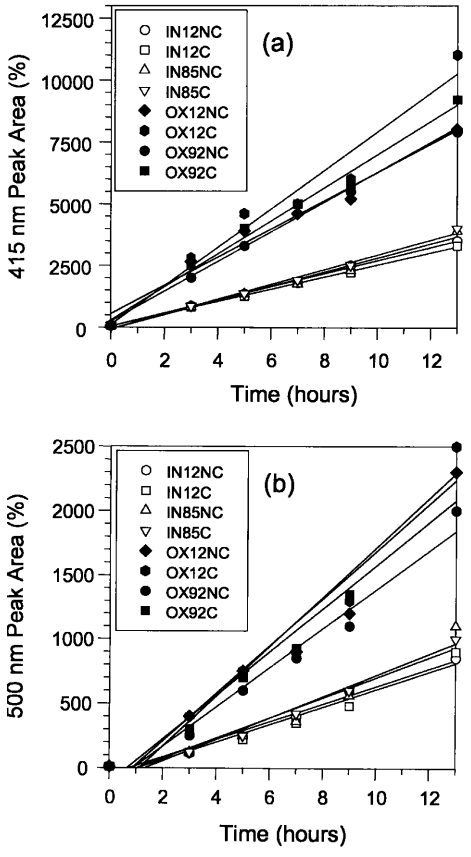

Fig. 11 Changes in **a** the 415-nm and **b** the 500-nm absorbance peaks (percent change) as a function of test time with linear regression for each test series. The linear relationships between peak areas and test time show that the absorption behavior is characteristic of the high-order kinetics reaction to form high-MW degradation products

Conclusions

The formation of high-MW, carbonaceous residue was investigated for a synthetic ester-based lubricant degraded in thermal and thermal–oxidative environments. Changes in viscosity, antioxidant content, acid content, and MW yielded insight into the onset of antioxidant depletion and the formation of high-MW degradation products. Using the Einstein equation for Newtonian fluids containing small particles, the high-MW species were found to act as discrete particulate materials with respect to the physical behavior of the oil. After the antioxidant had been depleted, the reaction to form the particulate degradation products was diffusion-limited.

The changes in the absorbance spectra for degraded oil samples were shown to be the result of changes in the behavior of three absorption peaks located at 355, 415, and 500-nm. As degradation proceeded, the 355-nm peak decreased in intensity and is thus attributed to the base lubricant, whereas the absorbances of the 415- and 500-nm peaks increased and are attributed to the particulate carbon degradation product. Furthermore, the 415-nm peak was attributed to an absorbance characteristic of the degradation product which reflects concentration, whereas the 500-nm peak was attributed to an absorbance characteristic which represents product concentration and size. The results demonstrate that optical absorption can be used for monitoring the formation of such particulate species in the synthetic lubricant.

Table 4 List of correlation coefficients and slopes for linear regression analysis performed on the absorbance versus time plots shown in Fig. 11

Test ID	415-nm peak: r^2	415-nm peak: slope	500-nm peak: r^2	500-nm peak: slope
IN12NC	0.998	265.2	0.980	68.1
IN12C	0.998	245.9	0.951	67.7
IN85NC	0.982	286.2	0.931	82.2
IN85C	0.991	298.6	0.970	77.7
OX12NC	0.975	571.0	0.957	186.5
OX12C	0.960	779.0	0.949	184.2
OX92NC	0.990	602.1	0.970	152.0
OX92C	0.987	669.3	0.952	192.6

Acknowledgements The authors gratefully acknowledge the support of the Air Force Office of Scientific Research Grant Number F49620-93-12-0349DEF, Pratt & Whitney for laboratory and equipment use in the West Palm Beach location, and the University for Florida, at which the investigation was centered.

References

1. Klaus EE, Duda JL, Wu WT (1991) Lubr Eng 47:679
2. Gee MG (1994) J Eng Tribol 208:153
3. Ajayi OO, Erdemir A, Hsieh JH, Erck RA, Fenske GR (1991) Lubr Eng 48:584
4. Hsu SM, Ku CS, Pei PT (1986) In: Stadtmiller WH, Smith AN (eds) Aspects of lubricant oxidation, ASTM STP 916. American Society for Testing. and Materials, Philadelphia, p 27
5. United Technologies, Pratt & Whitney (1988) The aircraft gas turbine engine and its operation, part no. P&W 182408
6. Hunter M, Klaus EE, Duda JL (1993) Lubr Eng 49:492
7. Schnabel W (1981) Polymer degradation principles and practical applications. Macmillan New York
8. Kauffman RE (1995) Lubr Eng 51:914
9. Haynes BS, Wagner HG (1981) Proc Energ Combust Sci 7:229
10. Kitamura K, Imada Y, Nakajima K (1993) Lubr Eng 49:185
11. KMontgomery DC (1991) Design and analysis of experiments, 3rd edn. Wiley, New York
12. Metals Hand Book, 9th Ed Volume 10: Materials characterization Copyright: American Society for metals 1986 Metals Park, Ohio, USA 44073
13. Rabek JF (1980) Experimental methods in polymer chemistry. Wiley, New York
14. Silverson RM, Bassler GC, Morrill TC (1991) Spectrometric identification of organic compounds, Wiley, New York
15. Einstein A (1956) Investigations on the theory of the brownian movement. Dover, USA
16. Overbeek JThG (1982) Adv Colloid Interface Sci 15:251
17. Hiemenz PC (1984) Polymer Chemistry Dekker, New York